# Inelastic-Neutron Scattering from bcc $^4$He†

E. B. Osgood,* V. J. Minkiewicz,‡ T. A. Kitchens, and G. Shirane
*Brookhaven National Laboratory, Upton, New York* 11973
(Received 29 October 1971)

Inelastic neutron scattering experiments were carried out on large single crystals of the quantum solid bcc $^4$He. The crystals were oriented in the [011] zone and had volumes larger than 5 cm$^3$. Both transverse and longitudinal excitations were studied with propagation vectors along the [100], [111], and [011] principal symmetry directions. Dispersion relations along these three symmetry directions are presented and discussed within the context of the results of recent theories for this highly anharmonic solid. The data, which present clear evidence for strong phonon relaxation, are also compared with theoretical linewidth estimates. The elastic constants calculated from these data are $c_{11}/\rho = 1.77 \pm 0.32$, $c_{12}/\rho = 1.58 \pm 0.35$, and $c_{44}/\rho = 1.07 \pm 0.10$ in units of $10^5$ m$^2$/sec$^2$, in good agreement with the results obtained from ultrasonic and thermodynamic measurements. When the amplitude of the scattering vector $|\vec{Q}|$ approaches $1.6a^* = 2.44$ Å$^{-1}$, where $a^*$ is the reciprocal-lattice vector of length 1.525 Å$^{-1}$, some extra intensity is observed near an energy of 1.4 meV. Evidence that this intensity is indeed real and anomalous, some four times as much as expected from single-phonon scattering, is presented. The physical origin of this extra scattering is not presently known.

## I. INTRODUCTION

An understanding of the physical properties of solid helium continues to be one of the most fundamental and interesting problems of physics. The interest in the solids of helium is derived from the fact that they are the most extreme examples of quantum solids. Quantum solids are characterized by having atoms with zero-point motions which are significant fractions of the lattice spacing. For solid helium, because of the very weak van der Waals interatomic forces and the light atomic masses, the zero-point motions in large molar volume samples are typically 30% of the lattice spacing. Because the interatomic potential is known reasonably well from second virial coefficient studies, a first-principles calculation of the physical properties of solid helium is possible. However, because of the large zero-point motion and the strong repulsive core of the interatomic interaction, the correlation of the atomic motions is extremely important in such a calculation and this remains a challenge to the theoretical understanding of the solid.

Without doubt, the most detailed information on the dynamics of solids is obtained from the phonon dispersion relation. There have been neutron diffraction studies of the hcp phase of $^4$He.[1,2] However, the bcc phase is a particular interest because of its high symmetry. Because there is only one atom in each unit cell, the data analysis is not complicated by the need to utilize inelastic structure factors. Unfortunately, the bcc phase of $^3$He, which exists over a wide range of pressures and temperatures, cannot be studied by neutron diffraction techniques because of its large absorption cross section. In this paper the phonon dispersion relation for the bcc phase of solid $^4$He is presented and compared with the calculations for the conditions of this experiment from several theories. The results of this work show that although much progress has been made in our understanding of the solids of helium, there is much yet to be understood.

A recent review of the theoretical work on the problem of quantum solids, including a bibliography, is given by Werthamer.[3] The classical methods[4] of lattice dynamics yield imaginary frequencies[5] and thus perturbation theories from a classical basis are impossible. A basis must be developed in a self-consistent way, where the potential is effectively averaged over the motions of the atoms in the crystal. A method should be used that includes, in a systematic and consistent manner, the short-range correlations that prevent the unphysical overlap of the wave functions at small interatomic separation, where the repulsion is large.

Recently, there have been several calculations of the lattice dynamics of bcc $^4$He. In the work of Glyde[6,7] the dispersion relations for bcc helium are calculated using a Green's-function technique. In the lowest-order or self-consistent harmonic (SCH) approximation developed earlier,[3] the basic low-energy excitations are assumed to be phonons. Effective spring constants and wave functions are determined in a self-consistent way. The short-range correlations are taken into account by introducing Jastrow functions and thereby producing an effective Hamiltonian. The form of the Jastrow function is that of Nosanow,[8] where the parameters are determined by minimizing the ground-state energy. In the next order of approximation (SCHC), the results of the SCH theory are used as a basis and the cubic terms in the expansion are treated

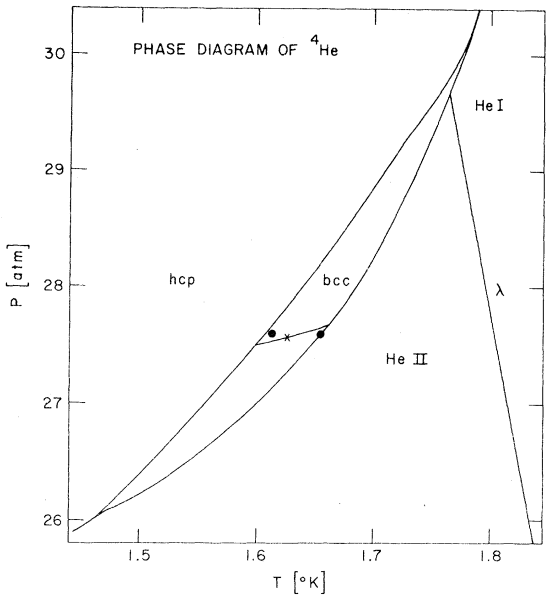


FIG. 1. Phase diagram of $^4$He near the bcc phase. The circles are the temperatures of the top and bottom of the cell during crystal growth. The cross is the temperature of the crystal after growth was completed. The curve through the cross is the isochore at $V_M = 21.00$ cc/mole.

as a perturbation.

More recently, Glyde and Khanna[9] have used a $T$-matrix approach to account for the short-range correlations. This method is similar to the work of Guyer[10] and Horner.[11] The real wave function is assumed to be related to the correlated Gaussian or harmonic wave function by a $T$ matrix. They consider a pair of atoms interacting with each other through the exact potential. The pair is in a double well determined by the interaction of its neighbors with the pair through an effective harmonic potential. The Schrödinger equation for the pair is solved for the $T$ matrix. The $T$ matrix is used to calculate the effective harmonic potential, which in turn determines the phonon frequencies and the $T$ matrix. The system of equations derived is iterated to provide a self-consistent set of quantities. As before, the cubic anharmonic term is included by perturbation theory by using the basis of the self-consistent wave functions calculated in the $T$ matrix approach.

Horner[11,12] has calculated the dispersion curves of bcc $^4$He using the techniques of many-body perturbation theory. The short-range correlations are taken into account in the manner described in Ref. 12. This method is closely related to that of Guyer.[10] For this calculation, the cubic anharmonic terms are included in a self-consistent way.

The calculation of Koehler and Werthamer[13] uses a variational technique with correlated Gaussian wave functions to find the phonon frequencies. The short-range correlations are accounted for by using an effective potential determined from a lowest-order cluster expansion with correlation functions of the Jastrow form. The effects of the higher-order anharmonicities are calculated by including two- and three-phonon modes in the variational basis set. All of the above treatments used the interatomic potential of Beck,[14] except Koehler and Werthamer, who used the Lennard-Jones potential.

As was pointed out by Werthamer,[15] because of the large zero-point motion in solid helium and thus the large Debye-Waller factor, the usual assumption that there is negligible contribution from the interference terms between the one-phonon peak and the multiphonon background is not valid. Thus one might expect to find neutron-scattering profiles with different shapes at equivalent positions in different Brillouin zones for helium. Indeed, in this experiment such effects were observed, in strong contrast with results from more classical solids.

Ambegaokar *et al.*[16] have derived a one-phonon sum rule that includes both the one-phonon scattering and the interference scattering between the one-phonon and the multiphonon background scattering. In this experiment, the scattered intensity from the bcc phase of $^4$He appears to strongly violate the sum rule even when allowances are made for the difficulties of removing the background. The extra intensity observed appears to be localized about a $\vec{Q}$ modulus of $1.6a^* = 2.44$ Å$^{-1}$ (where $\vec{Q}$ is the scattering vector and $a^*$ is the reciprocal-lattice vector of length 1.525 Å$^{-1}$) and an energy of approximately 1.4 meV.

Section II consists of a discussion of the experimental techniques used in this experiment, both the techniques of preparing a sample and the techniques for measuring the neutron scattering. The neutron-scattering results are presented in Sec. III. In Sec. IV the results are discussed and compared with the various theories, and Sec. V is a summary of the paper.

## II. EXPERIMENTAL TECHNIQUE

### A. Crystal Growth

The properties of helium make it difficult to grow and maintain a bcc crystal suitable for neutron-diffraction experiments. The reasons for this can be seen from the phase diagram of $^4$He shown in Fig. 1.

Because the bcc phase is, at most, 0.050 °K wide and 0.60 atm high, the temperature must be carefully regulated during the crystal growth and throughout the weeks required for the scattering experiment. During the crystal growth the heat of fusion must be removed through the grown crystal with a rate determined by the thermal conductivity of the crystal and the requirement that the crystal itself

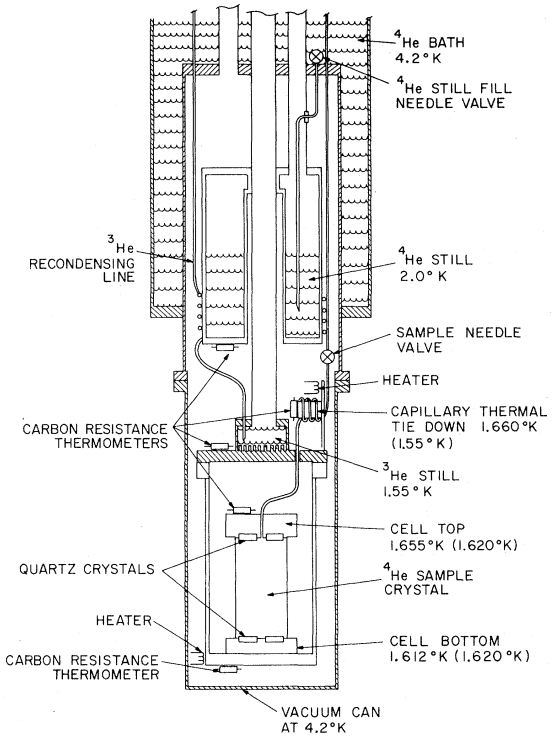


FIG. 2. Schematic representation of the cryostat used for this experiment. The temperatures indicated are typical values during crystal growth. The temperatures in parentheses are typical values after growth is completed.

remain in the bcc phase. Because of the poor thermal conductivity[17] of bcc $^4$He, 20–30 h are required to grow the 7.0-cm crystal used in this experiment. The poor thermal conductivity of the bcc helium has an additional consequence: If the heat input to the top of the crystal is too high (above 50 $\mu$W for our crystal with a cross-sectional area of 7.0 cm$^2$) the top of the crystal will melt if the bottom of the crystal is held within the bcc phase.

The cryostat used is shown in Fig. 2. It is a modification of the one used earlier[1] to study the hcp phase. The bottom of the cell is connected thermally to the $^3$He still by an aluminum thermal shield that surrounds the cell. The power into the heater at the bottom of the shield is servoed to keep the temperature at the carbon resistance thermometer constant to within 0.001 °K. The temperature at the $^3$He still is maintained constant to within 0.02 °K by regulating the vapor pressure over the $^3$He with a manostat. The $^4$He still is used to recondense the $^3$He returning to the $^3$He still in a closed system.

During the crystal growth the largest source of heat leaking into the cell is conduction through the superfluid liquid in the fill capillary.[18] This heat leak is maintained below 10 $\mu$W by using 20 cm of 0.01-cm-diam capillary filled with a 0.008-cm-diam wire. The temperature of the capillary is held within 0.005 °K of the melting temperature by controlling the power into the heater on the capillary thermal tiedown at the $^3$He still. After the crystal is grown the tiedown is cooled so that the capillary is full of solid, eliminating this source of heat.

The pressure is regulated during the crystal growth to within 0.02 atm. The difference between the pressure in the fill capillary and the pressure in a temperature-controlled reference volume is measured with a differential transducer. The output of the transducer is used to control the position of a piston in a cylinder in the fill line to maintain the pressure at a constant value. The position of the piston can be monitored to determine how much helium has entered the cell, and thus, how much helium has been converted from liquid to solid.

The crystals were grown from the superfluid phase at 27.60 atm with a temperature gradient of 0.042 ± 0.005 °K. The liquid sample at 27.60 atm was first precooled to just above the melting temperature. The $^3$He still is then cooled below the melting temperature and the temperature of the bottom of the cell is regulated just above the hcp-phase-transition temperature. When the cell cools below the melting curve, helium begins to go into the cell. The temperature of the top of the cell remains constant at the melting temperature for the 20–30 h that it takes to grow a crystal because there is no thermal gradient in the superfluid liquid phase. As the cell fills, the rate at which solid is formed decreases. When the cell is full, the needle valve in the fill line is closed and the crystal is maintained at constant volume at a temperature of 1.620 ± 0.005 °K.

Because the working point is so close to the phase boundary, care has to be taken to ensure that there is no liquid remaining in the cell. The completion of the crystal growth is indicated by the cooling of the top of the sample cell toward the temperature of the bottom of the cell. This cooling is not dramatic; it has a decay time of about 20 min. This is in agreement with the decay time of 25 min calculated using the measured specific heat[19] and thermal conductivity[17] of the bcc solid, for the geometry of our cell. If the cell contained any liquid, the decay time would be increased by a factor of 2 or more.

A conical cavity was drilled through the Epoxy that covered the bottom of the cell to the copper bottom of the cell in an attempt to provide a nucleation point and to encourage the growth of a single crystal. (It is, however, quite possible that the nucleation of crystal growth was on one of the four gold-coated quartz sound transducers on the cell bottom but they were more or less thermally insulated by their Epoxy substrate.) All eight of the crystals grown in this work had a [001] crystal direction within about 5° of each other. More than one-

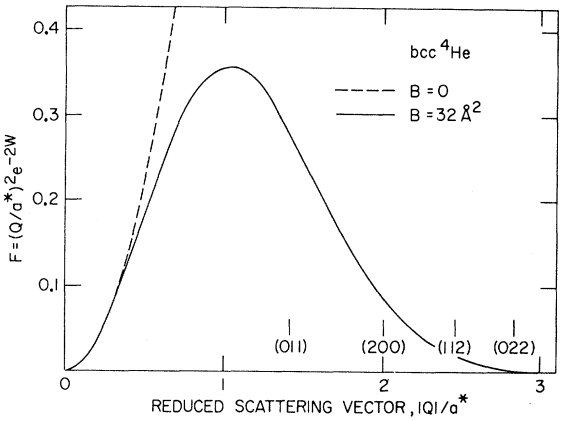


FIG. 3. Intensity factor due to the atomic motions is plotted as a function of reduced scattering vector $|\vec{Q}|/a^*$, where $a^*=2\pi/a=1.525$ Å$^{-1}$. The modulus of the scattering vector at several Bragg points is indicated. $B=W(2\pi/\vec{Q})^2=(3\hbar^2/2Mk\theta)$.

half of these had a [110] zone within 10° of the axis of the cell, which is also the growth axis.

Data were taken on three different crystals which were oriented in the [110] zone. In all cases, all the observed Bragg peaks corresponded to the crystal used and the reflected intensity had a profile roughly corresponding to the complete sample. Rough calculations showed, however, that the observed intensity could be expected from crystals as small as 5 cm$^3$. No exhaustive search was made for other Bragg peaks, but the beam was masked down to the observed profile to minimize other scattering, as explained in Sec. II B.

### B. Inelastic-Neutron Scattering

Neutron-scattering data were taken utilizing a triple-axis spectrometer operated in the constant-$\vec{Q}$ mode with a fixed incident neutron energy of 13.5 meV. The source of neutrons was the high-flux beam reactor located at Brookhaven National Laboratory. The effective beam collimation before and after the sample was 20 min. The majority of data collected in this experiment utilized neutrons that were monochromated and analyzed with the (002) reflection of a bent pyrolytic-graphite crystal.[20] However, in order to determine the effect on the position, shape, and relative intensities of selected phonon groups, a flat graphite analyzer was used. No effect on the phonon groups from the use of bent crystals was observed. The $\lambda/2$ component of the incident beam was effectively eliminated by a pyrolytic-graphite filter. In addition, special care was taken to mask the aperture of the analyzer and also the incident beam to the dimensions of the crystal being studied. This minimized the possibility of observing neutrons scattered by extraneous crystals in the sample chamber, if present, and otherwise reduced the background.

The lattice spacing of the bcc $^4$He crystals used in this experiment was observed to be $4.120\pm0.004$ Å. This value is in excellent agreement with the x-ray measurements[21] after suitable scaling with respect to the different molar volumes. This value is also in close agreement with that calculated from molar volume measurements.[22]

The relative intensities of the phonon groups assume a major role in the interpretation of the experimental results in the following sections of this paper. Pertinent to these interpretations is the procedure used to reduce the scattering data to account for the scattering properties of solid helium and the energy dependence of the efficiency of the analyzing system.

The scattering of neutrons by solid helium is severely curtailed by the large zero-point motion of the helium atoms. In the usual terms, the large zero-point motion causes the Debye-Waller factor to be quite small for the scattering vectors that are normally used in determining the phonon dispersion relation. This fact restricts the useful scattering in this experiment to the first and part of the second Brillouin zones and largely removes the possibility of observing a particular phonon group from more than one or, at most, two equivalent positions in reciprocal space. Mathematically, these points may be seen by considering the one-phonon cross section. This is proportional to $(\vec{Q}\cdot\vec{\xi})e^{-2W}$. Here $\vec{Q}$ is the scattering vector, $\vec{\xi}$ the phonon polarization vector, and $e^{-2W}$ is the Debye-Waller factor. The dependence of this factor on $\vec{Q}$ for bcc $^4$He is illustrated in Fig. 3 and clearly shows how $e^{-2W}$ limits the useful range. The value of $W$ is taken from an estimated $\Theta_D=22.5$ °K,[19] where $\Theta_D$ is the Debye temperature.

In order to scale the integrated intensity of the phonon groups, the spectrometer has been calibrated under identical conditions by using a copper single crystal as a sample. The known factors in the scattering cross section were divided out, which leaves the observed intensities for the copper crystal as a correction factor. This is a largely a reflection on the efficiency of the analyzer system. This energy-dependent correction factor was then applied to the scattering data from the bcc $^4$He crystals. The correction is less than 30% for energy exchange between 1.0 and 4.0 meV.

## III. RESULTS

The results of this experiment are to be presented in two parts. First, the data taken in the region of $|\vec{Q}|\sim1.6a^*$ ($a^*$ being the reciprocal-lattice vector $2\pi/\alpha=1.525$ Å$^{-1}$), where the anomalous extra intensity is seen, are discussed. Evidence that the additional intensity is indeed anomalous is presented in this section. However, information indicating that the

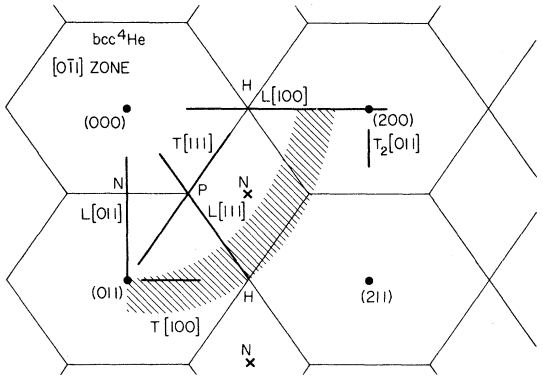


FIG. 4. [110] zone in reciprocal lattice space for a bcc structure. The dots indicate the Bragg peaks. The light lines indicate the Brillouin zone boundaries. The heavy lines indicate where data were taken for the various branches. Zone boundary data for the transverse [011] branches were taken at the $N$ points at the center of the Brillouin zone face indicated by ×. The shaded area indicates where large values of the "scaled intensity" were observed.

additional scattering is not an artifact is given in a latter section. Second, the results in which the scattered intensity appears to be normal are discussed and compared with recent theoretical calculations of both the dispersion and the phonon lifetimes.

### A. Anomalous Scattering

Inelastic-scattering data were collected along the symmetry directions in the regions indicated by the heavy lines shown in Fig. 4. The majority of the data indicated that the phonons, albeit heavily damped, behaved in normal manner. However, for those scans taken in or near the shaded region in the figure, strongly asymmetric scattering profiles were observed. For some scattering vectors this asymmetry was accompanied by an unexpected increase in scattered intensity. By additional intensity we mean that there was more than would be expected on the basis of the one-phonon sum rule derived by Ambegaokar *et al.*[16]

The development of the extra intensity and attendant asymmetry is most clearly illustrated by data taken along the $L[100]$ branch. Several phonon profiles along this branch are plotted in Fig. 5. The phonons measured in the first Brillouin zone at (0.5, 0, 0), (0.6, 0, 0), and (0.8, 0, 0) are symmetric, although broad, and can be fitted quite well with a Gaussian line shape. In the second zone at (1.2, 0, 0) and (1.5, 0, 0), asymmetric profiles are observed. The profiles for $|\vec{Q}| \geq 1.7a^*$ are again symmetric. Comparing the shapes at (0.8, 0, 0) and (1.2, 0, 0) and at (0.5, 0, 0) and (1.5, 0, 0), one sees that, contrary to what is observed in most other solids, the phonon profiles at equivalent positions in the first and second Brillouin zones are very different.

For a direct comparison of the shapes and the expected intensities, the data taken at (1.5, 0, 0) are plotted with the background subtracted in Fig. 6. The Gaussian fit to the (0.5, 0, 0) data is also plotted on the same figure. The amplitude is corrected for the difference in counting time and for the factor $\vec{Q}^2 e^{-2W}$. For $|\vec{Q}| = 0.5\alpha^*$, the profile is asymmetric and for $|\vec{Q}| = 1.5a^*$ there is more intensity than expected, as is seen in the figure. The profile with extra intensity is asymmetric with a sharp rise at low-energy transfer, and peaks around an energy of 1.4 meV, and thereafter slowly falls off at higher energies. This is also characteristic of most profiles with extra intensity. The same features are presented for phonon pronon profiles at $|\vec{Q}| \sim 1.6\alpha^*$ along other symmetry directions, such as the $L[111]$ and $T[100]$. Outside the shaded area, groups were observed with distorted profiles but without additional intensity.

In order to determine quantitatively the amount of extra intensity in these anomalous peaks, one can use the one-phonon sum rule.[16] The sum rule can be written

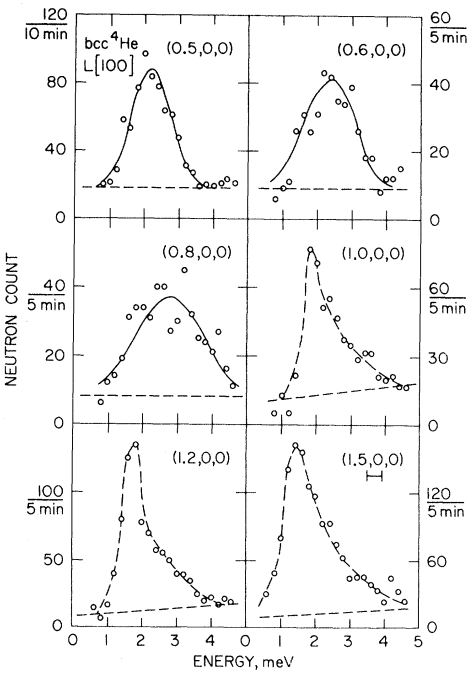


FIG. 5. Examples of phonon profiles for the $L[100]$ branch. The value of the reduced scattering vector $\vec{Q}/a^*$ is indicated. The solid lines represent Gaussian fits to the data. The straight dashed lines indicate estimates of background. The dashed lines through the data are drawn by eye. The FWHM due to instrumental resolution is indicated in the lower right-hand corner.

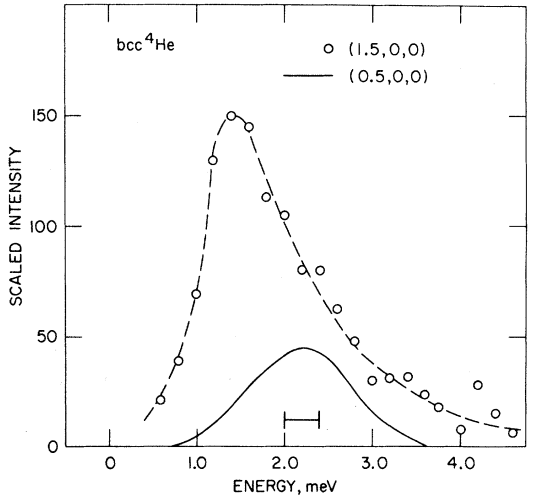


FIG. 6. $L[100]$ phonon profiles at the equivalent positions $\vec{Q}/a^* = (1.5, 0, 0)$ and $(0.5, 0, 0)$ are plotted. The background is subtracted and the intensities are corrected for Debye-Waller factor and counting rate. The instrumental resolution is indicated.

$$\frac{\int_0^\infty d\omega\, \omega S_p(\vec{Q}, \omega)(1 - e^{-\beta\omega})}{(\vec{Q}\cdot\vec{\xi})^2 e^{-2W}} = 1 , \qquad (1)$$

where $\beta = \hbar/kT$, $\vec{\xi}$ is the polarization vector of the phonon, $e^{-2W}$ is the Debye-Waller factor, and $S_p(\vec{Q}, \omega)$ is that part of the scattering function due to single phonons. It has been argued by Ambegaokar *et al.*[16] that this sum rule is valid in anharmonic crystals where $S_p(\vec{Q}, \omega)$ includes the interference terms between the single-phonon scattering and the multiphonon background.

This sum rule has been evaluated for our experimental data. A linear background, which is estimated by eye and from background measured on other scans where no phonon intensity is present, is first subtracted from the data. The data are then corrected for monitor counting rate and for the energy dependence of the spectrometer sensitivity, the appropriate integrations are performed, and the result is divided by $(\vec{Q}\cdot\vec{\xi})^2 e^{-2W}$. For those scans (e.g., at the point $N$) where two phonons are observed with perpendicular polarization vectors, the result was divided by $|\vec{Q}|^2 e^{-2W}$, since for this case $(\vec{Q}\cdot\vec{\xi}_1)^2 + (\vec{Q}\cdot\vec{\xi}_2)^2 = |\vec{Q}|^2$. The resulting "scaled intensity" should be independent of scattering vector and depend only on the spectrometer parameters such as sample size and geometry and collimations used. The scaled intensity is found to be independent of $|\vec{Q}|$ for $|\vec{Q}| \lesssim 1.2a^*$. The result for the various experimental conditions were thus normalized at low $|\vec{Q}|$. Using this procedure, the intensities of all of the measured phonon profiles can be compared.

The results are plotted in Fig. 7 as a function of $|\vec{Q}|/a^*$. As can be seen from the figure, the data for $|\vec{Q}| < 1.3a^*$ and $|\vec{Q}| > 1.7a^*$ are completely consistent. In data for which $|\vec{Q}| \approx 1.6a^*$, the additional intensity contributes as much as four times the "normal" value. The large scatter in the values of the scaled intensity is due to uncertainties in the value of the background. Representative estimated errors are indicated. That the extra intensity is not an artifact is proven by various checks that are described in Sec. IV.

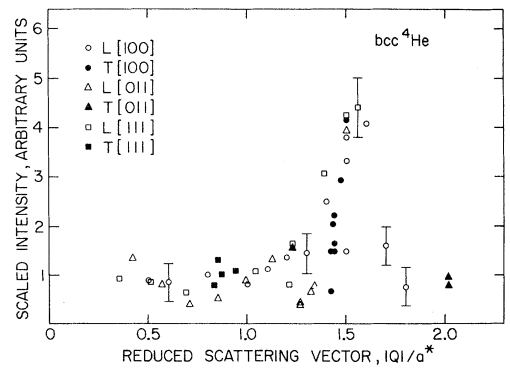


FIG. 7. Normalized value of the one-phonon sum rule, evaluated for many different experimental scans, is plotted vs the scattering vector. The error bars indicate estimates of typical errors.

### B. Phonon Dispersion and Relaxation

For most of the data collected with the scattering vector $\vec{Q}$, neither in nor near the shaded area in Fig. 4, the phonon groups observed were well defined and symmetric and had approximate Gaussian line shapes as well. Examples of these normal phonons are shown in Fig. 8. The data were first adjusted to account for the energy dependence of the efficiency of the energy analyzer. To parametrize the width and position of these phonon groups,

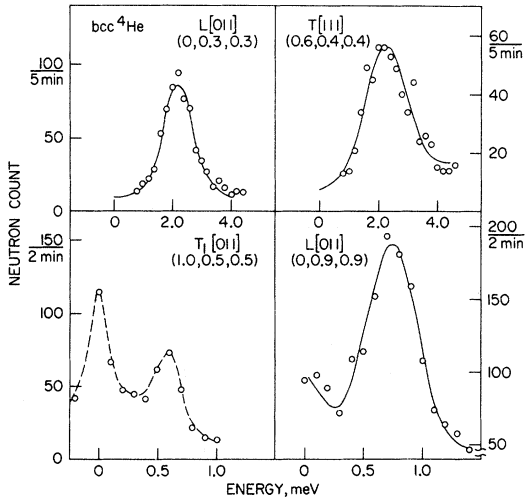


FIG. 8. Typical phonon profiles for scans with normal intensity.

TABLE I. Experimental peak positions and widths of phonons in bcc $^4$He.

| $\vec{q}/a^*$ | $\vec{Q}/a^*$ | $E$(meV) | FWHM(meV) |
|---|---|---|---|
| | | $L$[100] | |
| (0.2,0,0) | [1.8,0,0] | 0.80 ± 0.10[a] | |
| (0.3,0,0) | [1.7,0,0] | 1.45 ± 0.14[a] | |
| (0.5,0,0) | [0.5,0,0] | 2.24 ± 0.06 | 1.27 ± 0.14 |
| (0.6,0,0) | [0.6,0,0] | 2.50 ± 0.12 | 1.45 ± 0.24 |
| (0.8,0,0) | [0.8,0,0] | 2.95 ± 0.20 | 2.20 ± 0.35 |
| | | $T$[100] | |
| (0.1,0,0) | [0.1,1,1] | 0.345 ± 0.012 | 0 ± 0.14 |
| (0.15,0,0) | [0.15,1,1] | 0.521 ± 0.016 | $0.32^{+0.09}_{-0.12}$ |
| (0.2,0,0) | [0.2,1,1] | 0.63 ± 0.04 | $0.43^{+0.14}_{-0.17}$ |
| (0.25,0,0) | [0.25,1,1] | 0.85 ± 0.04 | 0.37 ± 0.06 |
| (0.3,0,0) | [0.3,1,1] | 0.93 ± 0.05 | |
| | | $L$[111] | |
| (0.1,0.1,0.1) | [0.1,1.1,1.1] | 0.98 ± 0.08[a] | |
| (0.2,0.2,0.2) | [0.2,0.2,0.2] | 1.87 ± 0.05 | 0.92 ± 0.14 |
| (0.3,0.3,0.3) | [0.3,0.3,0.3] | 2.51 ± 0.13 | 1.58 ± 0.28 |
| (0.4,0.4,0.4) | [0.4,0.4,0.4] | 2.32 ± 0.15 | 1.12 ± 0.30 |
| (0.5,0.5,0.5) | [0.5,0.5,0.5] | 2.14 ± 0.14 | 1.17 ± 0.26 |
| (0.7,0.7,0.7) | [0.7,0.7,0.7] | 1.29 ± 0.08 | 1.01 ± 0.18 |
| | | $T$[111] | |
| (0.1,0.1,0.1) | [0.1,0.9,0.9] | 0.25 ± 0.08[a] | |
| (0.2,0.2,0.2) | [0.2,0.8,0.8] | 0.74 ± 0.08[a] | |
| (0.6,0.6,0.6) | [0.6,0.4,0.4] | 2.33 ± 0.10 | 1.56 ± 0.2 |
| (0.8,0.8,0.8) | [0.8,0.2,0.2] | 2.50 ± 0.10 | 1.39 ± 0.2 |
| | | $L$[011] | |
| (0,0.05,0.05) | [0,0.95,0.95] | 0.312 ± 0.02 | 0.24 ± 0.12 |
| (0,0.07,0.07) | [0,0.93,0.93] | 0.488 ± 0.05 | 0 ± 0.1 |
| (0,0.1,0.1) | [0,0.9,0.9] | 0.73 ± 0.03 | 0.15 ± 0.15 |
| (0,0.15,0.15) | [0,0.85,0.85] | 1.2 ± 0.08[a] | |
| (0,0.2,0.2) | [0,0.8,0.8] | 1.64 ± 0.06 | $0.69^{+0.15}_{-0.17}$ |
| (0,0.3,0.3) | [0,0.3,0.3] | 2.25 ± 0.05 | 1.22 ± 0.12 |
| | [0,0.7,0.7] | 2.28 ± 0.10 | 1.19 ± 0.20 |
| (0,0.4,0.4) | [0,0.4,0.4] | 2.60 ± 0.14 | 1.40 ± 0.40 |
| | [0,0.6,0.6] | 2.55 ± 0.16 | 1.10 ± 0.40 |
| (0,0.5,0.5) | [0,0.5,0.5] | 2.75 ± 0.2 | 1.2 ± 0.3 |
| | | $T_1$[011] | |
| (0,0.5,0.5) | [1,0.5,0.5] | 0.6 ± 0.06[a] | |
| | | $T_2$[011] | |
| (0,0.2,0.2) | [2,0.2,0.2] | 0.91 ± 0.03 | $0.30^{+0.12}_{-0.20}$ |
| (0,0.3,0.3) | [2,0.2,0.2] | 1.22 ± 0.04 | 0.30 ± 0.14 |
| (0,0.5,0.5) | [1,0.5,0.5] | 1.47 ± 0.10[a] | |

[a]Evaluated by eye.

the peaks were approximated with a Gaussian line shape plus a linear background. The peak energies of the phonons are plotted in Fig. 9 and listed in Table I. The errors that are quoted are twice the statistical error from the curve-fitting procedure. There were a few points where the background was too difficult to estimate. For these data, the energy and errors in energy for the phonon peak were estimated by eye.

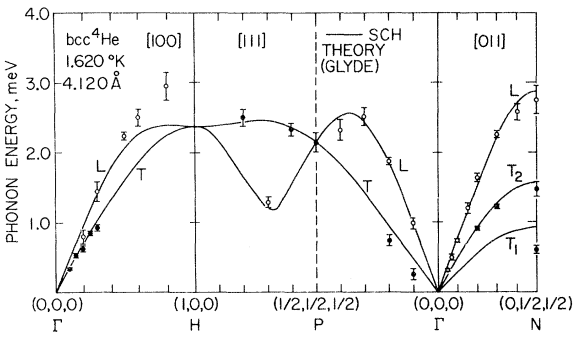


FIG. 9. Experimental dispersion curves for bcc $^4$He at 21.0 cm$^3$/mole. The solid dots indicate transverse branches. The open circles indicate longitudinal branches. The solid lines represent the first-order theory of Glyde (Ref. 7).

The widths of the phonon peaks were also determined from the curve-fitting procedure. The widths, given in Fig. 10 and Table I, were determined by taking the difference of the squares of the widths from the Gaussian fit and the instrumental resolution. The instrumental resolution was calculated for each point by using the slope of the dispersion curve from Fig. 9. The instrumental resolution was between 0.35 and 0.45 meV full width at half-maximum (FWHM) for all points. The errors quoted for the widths are again twice the statistical error from the curve-fitting procedure plus an assumed 5% error in the instrumental resolution. The energies and widths for only those phonon profiles that were symmetric and had intensities consistent with the one-phonon sum rule are presented in Figs. 9 and 10 and in Table I.

For the $L$[011] branch, there are two sets of data at equivalent positions in the first and second Brillouin zones at (0,0.3,0.3) and (0,0.7,0.7) and at (0,0.4,0.4) and (0,0.6,0.6). It must be emphasized that, in contrast with the $L$[100] data, the agreement

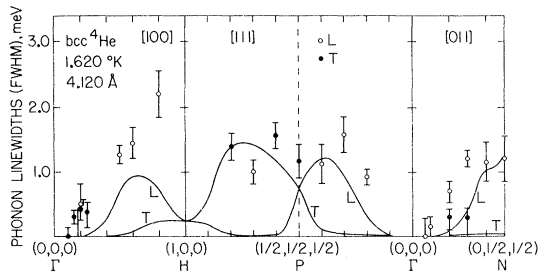


FIG. 10. Experimental FWHM of phonons in bcc $^4$He at 21.0 cm$^3$/mole. The solid dots indicate transverse branches and the open circles indicate longitudinal branches. The solid lines represent the results of the theory of Koehler and Werthamer (Ref. 13).

of the shapes, positions, and scaled intensities of data taken at these equivalent positions is excellent.

## IV. DISCUSSION

### A. Anomalous Scattering

The extra contribution to the sum rule is observed to be greatest near $|\vec{Q}| = 1.6a^*$. Where there is extra intensity, the profile peaks occur between 1.4 and 1.8 meV. The position of the peaks is relatively independent of $\vec{Q}$. The size and shape of the extra intensity also appears to be nearly isotropic.

Several additional experiments were performed to determine whether the extra scattered intensity was an artifact. A set of data was taken with an empty cell under conditions identical to those where the anomalous intensity was observed with the solid sample. No scattering was found. One can conclude that extraneous scattering due to either the spectrometer or the crystal can be ruled out. Multiple scattering appears to be an unlikely explanation of this phenomenon because the additional scattering was observed in many different directions and in several different samples.

In addition to the experiments described above, the possibility that there might have been some liquid He present was explored. This was considered a likely explanation since it was recognized that the anomalous scattering occurred for scattering vectors with approximately the same amplitude as the one at which the roton minimum is located. This possibility can be ruled out on thermodynamic grounds (see Sec. II A). Furthermore, for liquid helium near the melting curve under the pressure at which the sample was formed, the energy of the roton at the roton minimum is less than 0.7 meV.[23] This is much lower, almost a factor of 2 lower, than the energy of the extra intensity observed in the solid.

The possibility that some hcp phase existed in the sample and gave rise to the extra scattering was also virtually ruled out. The observed Bragg scattering was not consistent with the existence of any hcp phase. Further, the anomalous scattering was observed to have the same characteristics for several samples. The isotropic character, as well as the more-or-less unique $|\vec{Q}|$ of the extra scattering, is not characteristic of the normal hcp phase phonons.[1]

In scanning the elastic scattering, no powder pattern was observed for any of the samples used and thus the existence of large numbers of crystallites of any material and the attendant effects was excluded.

Although at the present time no explanation has been given for the extra scattering observed in this experiment, there are several possible mechanisms that come to mind. The first, since in this experiment the neutron always gave energy to the sample, is the creation of a vacancy. From NMR and specific-heat data in the bcc phase of $^3$He, the vacancy formation energy is greater than 1.4 meV.[24] On the other hand, a recent NMR experiment in dilute $^3$He-$^4$He solid solution suggests, by extrapolation to zero $^3$He concentration, that the formation energy in the pure $^4$He bcc phase is about 0.5 meV.[25] However, in the creation of a vacancy by a dynamic process such as neutron scattering, an interstitial $^4$He atom must also be created. In classical solids, this often requires four to six times as much energy as the creation of the vacancy. For a quantum solid, this energy has yet to be estimated. Nevertheless, even if the magnitude of the energy of the interstitial-vacancy creation were to agree, the requirement of a more-or-less unique $|\vec{Q}|$ is not clear.

A second possibility is the excitation of a preexisting vacancy, since they are quite numerous under the conditions of this experiment. Here, theory would predict a dispersion curve that resembles an optical phonon.[26] The requirement of the more-or-less unique $|\vec{Q}|$ for the extra scattering does not agree with the theory; in fact, this $|\vec{Q}|$ appears not to be commensurate with the reciprocal-lattice vector.

A third possibility is that the approximations used in calculating the Debye-Waller factor fail in quantum solids.[27] Further theoretical work is necessary before a detailed comparison is made, yet one expects that calculations will yield only $\vec{Q}$ dependence and not the sharp energy observed here. However, the interference effects discussed in the Introduction[15] coupled with an anomalous Debye-Waller factor could provide an explanation of the observations.[27]

A fourth possibility is some localized, yet cooperative, excitation.[28] Earlier, it has been pointed out that the excitation of this type in the liquid, the roton, does not have the energy observed here. Nevertheless, there is the possibility that an excitation of the roton type may have very different characteristics when embedded in a periodic lattice. Local, but cooperative, excitations of other kinds are yet to be considered.

### B. Dispersion Relations

The dispersion relation data are presented in Fig. 9. They are very similar to dispersion relations in other bcc solids with some notable exceptions. A striking result is the high energy for the $L[100]$ branch at wave vectors near the zone boundary. A measurement was made at the zone boundary of the $L[100]$ branch and is illustrated in Fig. 5. However, because of its asymmetric profile, no unique energy could be assigned to it.

The solid curve in Fig. 9 is the result of a theoretical calculation based on the SCH approximation due to Glyde.[6,7] It is chosen as a guide to the eye

because it fits the data well. This agreement is probably fortuitous because higher-order corrections and more sophisticated theoretical approaches tend to provide less agreement. For instance, the corrections to this theory due to third-order terms are known to be large and tend to lower the phonon energies.

The results of the various theories agree with each other within 20–30%. The shape of the dispersion curves from the various calculations is similar to Glyde's SCH curve except along the $L[100]$ branch. For all of the theories that account for the cubic terms and the short-range correlations, this branch is depressed near the zone boundary to such an extent that the $L[100]$ branch crosses the $T[100]$ branch. However, it is only this branch that our data is in major disagreement with the theories.

For a detailed comparison of the theoretical calculations with the experimental results, the energies of selected phonons are listed in Table II. The agreement with Glyde's SCH + C theory is good along the [011] modes and for the [100] modes at low $\vec{q}$. The [111] modes are 10–20% below the data. For Glyde and Khanna's work, the $L[011]$ branch is low, although the agreement with the transverse branches is good. Again, the $L[111]$ modes tend to lie 20–30% below the data and the $L[100]$ mode at low $\vec{q}$ is low also. The $T[100]$ mode at low $\vec{Q}$ is in good agreement with the data. For Horner's calculation, the $L[011]$ mode is low and the $T_2[011]$ is high, while the $T_1[011]$ mode is in agreement with the data. The [111] modes are generally a little low. Koehler and Werthamer's results[13] tend to be 10–20% greater than the experimental data along the $L[011]$ and $T_2[011]$ modes and low by 10% for the [111] modes.

The requirement of degeneracy of the phonons at point $H$ implies that at least one of the phonon modes must have a very peculiar energy dependence. Neutron groups have been observed nearer and even at point $H$ (see Fig. 5), but have not been included in Fig. 9 because they do not fulfill our criterion of energy symmetry.

There are five branches, $L[100]$, $T[100]$, $L[011]$, $L[111]$, and $T[111]$ for which there are data at low wave vector. Using the data for $|\vec{q}|/\alpha^*$ less than 0.35, we fitted the data to a straight line through the origin. The squares of these five slopes were fitted using a least-squares procedure to obtain the three elastic constants: $C_{11}/\rho = 1.77 \pm 0.32$, $C_{12}/\rho = 1.58 \pm 0.35$, and $C_{44}/\rho = 1.07 \pm 0.10$. These values are in good agreement with the values $C_{11}/\rho = 1.73 \pm 0.26$, $C_{12}/\rho = 1.52 \pm 0.26$, and $C_{44}/\rho = 1.23 \pm 0.05$, in units of $10^5$ m$^2$/sec$^2$, obtained by Wanner[29] from an analysis of the transverse sound data of Lipschultz and Lee[30] and compressibility[22,30] and specific-heat data.[31,32] These values are also consistent with the longitudinal sound velocities on unoriented crystals of 540–555 m/sec seen by Vignos and Fairbank.[33] If these elastic constants are used to calculate the sound velocities for all of the modes, the agreement with the data is good except along the $T[111]$ mode where the two data points lie well below the expected values.

### C. Relaxation Effects

The phonon profiles that we observe are, in general, very broad and symmetric. The FWHM intensity is not infrequently a large fraction of the energy of the phonon. These observed phonon group widths indicate that relaxation effects cause many of the phonons to damp out in only a few cycles.

In Fig. 10, the data are compared directly with the result of the theory of Koehler and Werthamer.[13] Considering the state of the theory, the agreement is good. The major discrepancies appear to be at the $L[100]$ mode at $\vec{Q}/a^* = (0.8, 0, 0)$ and the $L[111]$ point at $\vec{Q}/a^* = (0.7, 0.7, 0.7)$. The $L[111]$ point at $(0.7, 0.7, 0.7)$, although the shape is symmetric and the intensity is normal, has $|\vec{Q}|/a^*$ near 1.4 and may be bollixed by the anomalous scattering.

The theory of Glyde[6] predicts widths for the phonons with a $\vec{q}$ dependence similar to that of Koehler and Werthamer but four times smaller than the observed results. Glyde and Khanna[9] predict widths two times less than Koehler and Werthamer's except along the [100] where their widths are nearly the same, and therefore generally a factor of 2 less than observed. Horner's calculations[12] yield a double-peaked spectral response for the $L[100]$

TABLE II. Comparison of theories with experiment for selected points on the dispersion curves of phonons in bcc $^4$He.

| Branch | $\vec{q}/a^*$ | Expt. | SCH Glyde | SCH + C Glyde | SCH + C Glyde and Khanna | SCH + C Horner | SCH + C Koehler and Werthamer |
|---|---|---|---|---|---|---|---|
| $L$ [011] | (0, 0.5, 0.5) | 2.75 ± 0.20 | 2.87 | 2.71 | 2.58 | 2.50 | 3.23 |
| $T_2$ [011] | (0, 0.5, 0.5) | 1.47 ± 0.10 | 1.57 | 1.43 | 1.61 | 1.68 | 1.67 |
| $T_1$ [011] | (0, 0.5, 0.5) | 0.60 ± 0.06 | 0.92 | 0.62 | 0.61 | 0.57 | 0.65 |
| $L$, $T$ [111] | (0.5, 0.5, 0.5) | 2.14 ± 0.14 | 2.16 | 1.99 | 1.73 | 1.83 | 1.90 |
| $L$ [111] | (0.7, 0.7, 0.7) | 1.29 ± 0.08 | 1.227 | 0.93 | 1.08 | 1.31 | 1.08 |
| $L$ [100] | (0.8, 0, 0) | 2.95 ± 0.20 | 2.38 | 2.01 | 2.05 | 2.14 | 2.39 |

phonon at (0.75, 0, 0). The secondary peak in the phonon profile at higher energy falls at about the energy that we observe for the $L(0.8, 0, 0)$ phonon. Within experimental resolution, no distinct double-peaked profiles were observed.

## V. CONCLUDING REMARKS

The lattice dynamics of the bcc phase of $^4$He has been studied by inelastic neutron scattering from single crystals. It was found to be decidedly more nonclassical than had heretofore been expected. It was observed that for particular scattering vectors, namely, those in the region for which $|\vec{Q}| \simeq 1.6a^*$, the scattering properties of the lattice cannot be described as scattering from a single-phonon state plus its interference with the multiphonon background. The additional cross section observed in the anomalous region is not contained in the "one-phonon," or first moment, sum rule found by Ambegaokar *et al.*[16] (see Fig. 7). In addition to the intensity anomaly, the profiles of most groups that were collected in the second zone were found to be highly asymmetric (see, for example, Figs. 5 and 6). The shape of these profiles can be described as having a sharp initial shoulder with a gradual falling off at the higher energies. It is clear that our interpretation of these asymmetric groups must await furthe detailed calculation of the spectral function itself.

The data that were collected in the first zone, on the other hand, could be interpreted in the usual manner; that is, one could establish that the groups had a well-defined energy and a unique width. The data in the first zone, along with selected data taken in the second, were used to construct dispersion curves (see Fig. 9). There existed a number of theoretical calculations, within various approximations, with which the data could be compared. Condensing the conclusion drawn from these comparisons, it can be said that, over-all, the agreement was of the order of $\pm 10\%$, except in the [100] direction for wave vectors in the vicinity of the zone boundary.

Although improved theoretical calculations are clearly necessary, the present agreement should be regarded as good. The data indicate that there also exists a strong wave-vector-dependent relaxation (see Fig. 10). Near the origin of the zone, the excitations are well defined; however, with increasing propagation vector they become more heavily damped until, in most cases, the natural linewidth becomes approximately equal to its energy. The data were compared with the results of a calculation by Koehler and Werthamer[13] and the agreement was found to be reasonable.

Clearly, more experimental work must be done. The most important is a more complete characterization of the behavior of the unusual extra cross section in the anomalous region. The origin of this additional scattering is not known at the present time. In view of the great care that was exercised in establishing its existence, we are convinced that its explanation will constitute a significant step in our understanding of the excitations in a quantum solid.

## ACKNOWLEDGMENTS

We wish to acknowledge many workers who have given us their thoughts and calculations concerning the quantum solid discussed here. N. R. Werthamer, T. Koehler, H. Glyde, and H. Horner have all contributed to our knowledge in this way. We would also like to acknowledge conversations with and aid from our colleagues at Brookhaven National Laboratory, especially M. Blume, P. P. Craig, V. J. Emery, E. P. Lipschultz, and L. Passell. Without the very able assistance of T. Oversluizen and M. Rosso this experiment would not have been possible.

---

†Work performed under the auspices of the U. S. Atomic Energy Commission.

*Present address: Stevens Institute of Technology, Hoboken, New Jersey 07030.

‡Present address: University of Maryland, College Park, Maryland 20742.

[1]V. J. Minkiewicz, T. A. Kitchens, F. P. Lipschultz, and G. Shirane, Phys. Rev. 174, 267 (1968). Equation (11) should read $W = (3\hbar^2/2m\Theta)(Q/4\pi)^2$. Also F. P. Lipschultz, V. J. Minkiewicz, T. A. Kitchens, G. Shirane, and R. Nathans, Phys. Rev. Letters 19, 1307 (1967).

[2]R. A. Reese, S. K. Sinha, T. O. Brun, and C. R. Tilford, Phys. Rev. A 3, 1688 (1971); T. O. Brun, S. K. Sinha, C. A. Swenson, and C. R. Tilford, in *Neutron and Inelastic Scattering VI* (International Atomic Energy Agency, Vienna, 1968).

[3]N. R. Werthamer, Am. J. Phys. 37, 763 (1969).

[4]M. Born and K. Huang, *Dynamical Theory of Crystal Lattices* (Oxford U. P., London, 1954).

[5]F. W. de Wette and B. R. A. Nijboer, Phys. Letters 18, 19 (1965).

[6]H. R. Glyde, Can. J. Phys. 49, 761 (1971).

[7]H. R. Glyde, J. Low Temp. Phys. 3, 559 (1970); and private communication, based on Ref. 6.

[8]L. H. Nosanow, Phys. Rev. 146, 120 (1966).

[9]H. R. Glyde and F. C. Khanna, Can. J. Phys. 49, 2997 (1971).

[10]R. A. Guyer, *Solid State Physics* (Academic, New York, 1969), Vol. 23, 413; Solid State Commun. 7, 315 (1969); R. A. Guyer and L. I. Zane, Phys. Rev. 188, 445 (1969).

[11]H. Horner, Phys. Rev. A 1, 1722 (1970).

[12]H. Horner, Z. Physik 242, 432 (1971); and private communication.

[13]T. R. Koehler and N. R. Werthamer, Phys. Rev. A 3, 2074 (1971); and private communication.

[14]D. E. Beck, Mol. Phys. 14, 311 (1968).

[15]N. R. Werthamer, Phys. Rev. A 2, 2050 (1970).

[16]V. Ambegaokar, J. M. Conway, and G. Baym, J. Phys. Chem. Solids Suppl. 1, 261 (1965); in *Proceedings of the International Conference on Lattice Dynamics* (Pergamon, New York, 1965).
[17]B. Bertman, H. A. Fairbank, C. W. White, and M. Crooks, Phys. Rev. 142, 74 (1966); R. Berman and S. J. Rogers, Phys. Letters 9, 115 (1964).
[18]B. Bertman and T. A. Kitchens, Cryogenics 8, 36 (1968).
[19]B. J. Alder, W. R. Gardner, J. K. Hoffer, N. E. Phillips, and D. A. Young, Phys. Rev. Letters 21, 732 (1966); J. K. Hoffer, Ph. D. thesis (University of California, Berkeley, 1968) (unpublished).
[20]T. Riste, Nucl. Instr. Methods 86, 1 (1970).
[21]A. F. Schuch and R. L. Mills, Phys. Rev. Letters 8, 469 (1962).
[22]E. R. Grilly and R. L. Mills, Ann. Phys. 18, 250 (1962).
[23]O. W. Dietrich, E. H. Graf, C. H. Huang, and L. Passell (private communication); and unpublished.
[24]W. A. Reich, Phys. Rev. 129, 630 (1963); P. M. Richards, *ibid.* 137, A1327 (1965); E. C. Welmetes and C. A. Swenson, *ibid.* 128, 1512 (1962).
[25]R. C. Richardson (private communication).
[26]R. A. Guyer, R. C. Richardson, and L. I. Zane, Rev. Mod. Phys. 43, 532 (1971).
[27]N. R. Werthamer (private communication).
[28]A. F. Andreev and I. M. Lifshitz, Zh. Eksperim. i Teor. Fiz. 56, 2057 (1969) [Sov. Phys. JETP 29, 1107 (1969)].
[29]R. Wanner, Phys. Rev. A 3, 448 (1971).
[30]F. P. Lipschultz and D. M. Lee, Phys. Rev. Letters 14, 1017 (1965).
[31]D. O. Edwards and R. C. Pandorf, Phys. Rev. 144, 143 (1966).
[32]G. Ahlers, Phys. Rev. Letters 10, 439 (1963); Phys. Rev. 135, A10 (1964).
[33]J. H. Vignos and H. A. Fairbank, Phys. Rev. 147, 185 (1966).

PHYSICAL REVIEW A VOLUME 5, NUMBER 3 MARCH 1972

# Corrections to the Impulse Approximation for High-Energy Neutron Scattering from Liquid Helium*

H. A. Gersch, L. J. Rodriguez, and Phil N. Smith
*School of Physics, Georgia Institute of Technology, Atlanta, Georgia* 30332
(Received 4 October 1971)

Corrections to the impulse approximation for scattering from a many-body system are derived in the form of a series in inverse powers of the momentum transfer $k$. The coefficients in this series are written in terms of the two-body interaction potential and the particle-density matrices. Application is made to the case of high-energy neutron scattering from liquid helium. Evaluation of correction terms corresponding to a single helium-helium collision during the neutron-helium interaction time indicates (a) a shift in the peak of the incoherent-scattering cross section toward lower energy by a constant amount, and (b) an asymmetry of the cross section with respect to neutron energy loss about its peak value. Numerical estimates are given for these two effects for $k = 14.3$ Å$^{-1}$. Evaluation of condensate broadening due to multiple He-He collisions shows that the condensate-scattering contribution has a width proportional to $k^{1/2}$, and is thus distinguishable from the main noncondensate peak whose width is proportional to $k$. Estimates are given for requirements on experimental-resolution functions necessary to preserve this evidence of a distinct condensate contribution.

## I. INTRODUCTION

The inelastic cross section for neutrons on $He^4$ liquid is given in the Born approximation[1] by

$$\frac{d^2\sigma}{d\Omega\, d\epsilon_f} = \frac{\sigma_b k_f}{4\pi\hbar k_i} S(k,\ \omega)\ , \tag{1}$$

where $\hbar\vec{k} = \hbar\vec{k}_i - \hbar\vec{k}_f$ is the momentum transferred to the helium, $\hbar\omega = \epsilon_i - \epsilon_f$ is the energy transfer, and $\sigma_b = 1.13$ b.[2] The dynamic structure factor $S(k,\ \omega)$ is the Fourier transform of the density-density correlation function $S(k,\ t)$:

$$2\pi S(k,\ \omega) = \int_{-\infty}^{\infty} dt\, e^{-i\omega t} S(k,\ t)\ , \tag{2}$$

where

$$NS(k,\ t) = \sum_{j,l} \langle e^{-i\vec{k}\cdot\vec{r}_l(0)} e^{i\vec{k}\cdot\vec{r}_j(t)} \rangle\ . \tag{3}$$

The average value of the time-dependent density-density correlation function in Eq. (3) is in general taken over a canonical ensemble in equilibrium at temperature $T$. In the present work, we will restrict ourselves to $T = 0$. Equation (3) contains the Heisenberg operator $\vec{r}_j(t)$ defined for all $j$ and $t$ by